Environmental Pollution 272 (2021) 116022

Contents lists available at ScienceDirect

Environmental Pollution

journal homepage: www.elsevier.com/locate/envpol

Uranium removal from aqueous solution using macauba endocarp-derived biochar: Effect of physical activation☆

Sabine N. Guilhen [a, *], Suzimara Rovani [a], Leandro G. de Araujo [a], Jorge A.S. Tenório [b], Ondřej Mašek [c]

[a] Instituto de Pesquisas Energéticas e Nucleares, Comissão Nacional de Energia Nuclear, Av. Professor Lineu Prestes, 2242 – 05508-000, São Paulo, Brazil
[b] Depto. de Engenharia Química da Escola Politécnica, Universidade de São Paulo, Rua do Lago, 250 – 05508-080, São Paulo, Brazil
[c] UK Biochar Research Centre, School of Geosciences, University of Edinburgh, Alexander Crum Brown Road, Crew Building, EH9 3LA, Edinburgh, UK

ARTICLE INFO

Article history:
Received 25 June 2020
Received in revised form
16 September 2020
Accepted 5 November 2020
Available online 10 November 2020

Keywords:
Biochar
Activation
Macauba
Endocarp
Uranium

ABSTRACT

The main aim of this study was to evaluate options for addressing two pressing challenges related to environmental quality and circular economy stemming from wastage or underutilization of abundant biomass residue resources and contamination of water by industrial effluents. In this study we focused on residues (endocarp) from Macaúba palm (*Acrocomia aculeata*) used for oil production, its conversion to activated biochar, and its potential use in uranium (U) removal from aqueous solutions. Batch adsorption experiments showed a much higher uranyl ions (U(VI)) removal efficiency of activated biochar compared to untreated biochar. As a result of activation, an increase in removal efficiency from 80.5% (untreated biochar) to 99.2% (after activation) was observed for a 5 mg L^{-1} initial U(VI) concentration solution adjusted to pH 3 using a 10 g L^{-1} adsorbent dosage. The BET surface area increased from 0.83 to 643 m^2 g^{-1} with activation. Surface topography of the activated biochar showed a very characteristic morphology with high porosity. Activation significantly affected chemical surface of the biochar. FTIR analysis indicated that U(VI) was removed by physisorption from the aqueous solution. The adsorbed U(VI) was detected by micro X-ray fluorescence technique. Adsorption isotherms were employed to represent the results of the U adsorption onto the activated biochar. An estimation of the best fit was performed by calculating different deviation equations, also called error functions. The Redlich-Peterson isotherm model was the most appropriate for fitting the experimental data, suggesting heterogeneity of adsorption sites with different affinities for uranium setting up as a hybrid adsorption. These results demonstrated that physical activation significantly increases the adsorption capacity of macauba endocarp-derived biochar for uranium in aqueous solutions, and therefore open up a potential new application for this type of waste-derived biochar.

Credit author statement

Sabine Neusatz Guilhen: Conceptualization, Methodology, Validation, Formal analysis, Investigation, Data curation, Writing - original draft, Project administration, Funding acquisition. Suzimara Rovani: Formal analysis, Data curation, Writing - original draft, Visualization. Leandro Goulart de Araujo: Data curation, Writing - review & editing, Visualization. José Alberto Soares Tenório: Resources, Writing - review & editing, Funding acquisition. Ondřej Mašek: Conceptualization, Methodology, Writing - original draft, Visualization, Supervision.

1. Introduction

Activated carbon can be defined as an amorphous solid of high porosity and high specific surface area. Well-known adsorbents of widespread use, activated carbons have many applications, including purification and remediation of polluted water, treatment of liquid and gaseous industrial effluents, gas storage and delivery (methane and hydrogen), metal recovery, catalysis, and biomedical applications, among others (Bandosz, 2006; Bansal and Goyal, 2005; De Celis et al., 2009; Kwiatkowski, 2011; Le Cloirec and

☆ This paper has been recommended for acceptance by Yong Sik Ok.

* Corresponding author.
E-mail addresses: snguilhen@ipen.br (S.N. Guilhen), suzirovani@gmail.com (S. Rovani), lgoulart@alumni.usp.br (L.G. Araujo), jtenorio@usp.br (J.A.S. Tenório), ondrej.masek@ed.ac.uk (O. Mašek).

https://doi.org/10.1016/j.envpol.2020.116022
0269-7491/

Faur-Brasquet, 2008; Marsh and Reinoso, 2006; Mezohegyi et al., 2012; Nunell et al., 2012; Ramanujan et al., 2007; Rivera-Utrilla et al., 2011; Wang and Kaskel, 2012). Growing concerns surrounding environmental pollution have led to an increased demand for activated carbon in water treatment and sewage treatment applications. The global activated carbon market size was estimated at USD 4.72 billion in 2018 and it is expected to expand at a compound annual growth rate of 17.5% between 2019 and 2025 (Grand View Research, 2019; Roman et al., 2013).

The properties of activated carbon depend on the nature of the raw material used, the type of activation agent and the conditions of both the pyrolysis process and the activation itself. Characteristics such as shape, particle size, pore-volume, surface area, microporous structure, pore size distribution, physical and chemical characteristics of the surface define the properties and applicability of the activated carbon produced. It is possible to obtain different types of activated carbon with the modification of these parameters, making them more specific for a particular use (Rocha et al., 2006).

As a result of oxidation of surface functional groups, activated carbons typically have a non-polar or weakly polar surface (Yang, 2013). This way, it is widely used to purify, detoxify, deodorize, filter, discolor and remove a range of liquid and gaseous materials.

Almost all solid carbonaceous material can be converted to activated carbon. However, some characteristics must be taken into account when choosing the raw material, such as carbon content. The raw material must be high in carbon and low in inorganic matter (ash). Other important factors are the cost and availability of the raw material. Recently, agricultural residues have aroused a great deal of interest in the production of activated biochar, because they originate from renewable and low-cost resources (Chen et al., 2011; Kalderis et al., 2008). In this way, agricultural residues that would be normally discarded gained a new potential for usability, being transformed into valuable products, such as activated carbons.

The process of production of activated carbon typically involves three steps: the preparation of the raw material, carbonization, and activation. In each of these steps, the control of the operational conditions is decisive for the structural properties of the final product.

Preparation of raw material consists of removing any dirt or foreign residue that does not belong to the material. It also involves steps of grinding, for highest homogeneity during thermal decomposition, and oven-drying in advance of carbonization.

Carbonization consists of thermal treatment (pyrolysis) of the precursor material (raw material) in an inert atmosphere, at a temperature above 200 °C. In this step, the volatile components and light gases (CO, H_2, CO_2 and CH_4) are removed, leaving behind a porous carbon structure amenable to subsequent activation (Claudino, 2003). Biochars obtained from lignocellulosic materials are essentially microporous. However, these pores are often fully or partially filled by thermal decomposition products, such as tar (Rodriguez-Reinoso and Silvestre-Albero, 2016). Activation promotes the removal of organic compounds as well as other residues that can obstruct the pores of the biochar, forming sites with enhanced adsorptive capacity (Rocha et al., 2006).

The activation process impacts on the basic characteristics of the material, such as pore distribution and volume, density, specific surface area, and mechanical strength. Activation exposes the aromatic groups to the oxidizing agents and initiates the development of the microporous structure, characterizing the first phase of the process. In the second phase, the decomposition of the walls among adjacent pores promotes pore increase and the creation of large pores (Yang, 2013).

Activation can be carried out by chemical and physical processes. Chemical activation relies on the action of inorganic additives, such as H_3PO_4, HNO_3, $ZnCl_2$, H_2SO_4, NaOH, among others, to degrade and dehydrate the lignocellulosic material and, simultaneously, inhibit contraction during carbonization (Mestre and Carvalho, 2018). It consists of the impregnation of these activating agents into the not yet carbonized material. The impregnated material is then carbonized (between 400 and 800 °C) in the absence of oxygen (Contescu et al., 2018).

Activating agents generally have a dehydrating property, providing the formation of crosslinks, rendering the material less prone to volatilization when heated to elevated temperature. In this way, the formation of bituminous compounds inside the pores is inhibited. The product is cooled and washed to remove the remainder of the activating agent. In calcination, the chemical agents dehydrate the carbonaceous matter, resulting in the creation of the pores. Peng et al. (2017) managed to enhance Cu(II) and Cd(II) adsorption by modifying biochars with H_3PO_4. Trakal et al. (2014) used KOH activating agent to enhance Cu(II) adsorption onto brewers draft biochar. Hadjittofi and Pashalidis (2015) used HNO_3 oxidation in cactus fibers biochar for U(VI) adsorption from aqueous solutions. Wu et al. (2020) used Fe(II, III) modified rice straw-derived biochar in soils to retain phosphorous. The authors found that the adsorption capacity of Fe(II)-biochar was 2.4 times higher than biochar without any Fe. Recently, Teng et al. (2020) employed pinecone biochar as an adsorbing material. They found that this material has great potential to adsorb Cd(II), reaching a maximum of 92.7 mg g^{-1} of capacity. The review from Xiong et al. (2019) highlighted that biochar is considered an emerging low-cost adsorbent, already been used to remove toxic elements such as Cr, Cu, As, and Pb from water sources.

Physical activation, also called thermal activation, is the process of slow oxidation of the char, through which it develops a porous structure, increasing its surface area. This type of activation is performed after the carbonization process at a temperature between 700 and 1000 °C under appropriate flow of oxidizing gas (water steam or CO_2, used individually or in combination). This process is also known as partial gasification (Schettino Junior, 2004).

After physical or chemical activation, the activated biochar is subjected to subsequent steps, such as cooling, sieving, washing, drying, polishing, granulometric separation and packing.

Although chemical activation provides a greater yield, since it employs lower temperatures and shorter activation time (Maciá-Agulló et al., 2004), the cost of activating agents, combined with the additional washing step, may favor the use of physical activation. The advantages of physical activation are the possibility of developing a more porous structure with a larger active area, besides having a smaller environmental impact in terms of secondary pollution generation. Rajapaksha et al. (2015) reported the enhanced removal of sulfamethazine (SMT) from water by steam-activated biochar synthesized from an invasive plant (*Sicyos angulatus* L.). Franciski et al. (2018) used CO_2 activated biochar from solid wastes of a beer industry for methylene blue adsorption. As reported by Zhang et al. (2019), sludge-based biochar activated with CO_2 enhanced Pb(II) adsorption.

Activation is an essential tool for the production of biochar with higher specific surface area and highly developed porosity, promoting the increase in the adsorption capacity (Gorgulho et al., 2008). In the process of activation, it is desirable to obtain a product with high internal surface area. In general, the product of activation presents a large total pore volume and a high internal surface area in the range between 300 and 2500 m^2 g^{-1} (Yang, 2013).

Water molecules are much smaller than CO_2 molecules, which facilitates vapor diffusion through the porous network. As a result,

steam activation yields both micropores and mesopores with a wider range of pore size distribution, whereas CO_2 activation essentially forms and widens micropores (Dalai and Azargohar, 2007; Feng et al., 2018). Also, CO_2 activated biochar tends to be more thermally stable (Molina-Sabio et al., 1996).

IEA-R1, the largest research nuclear reactor in Brazil, is located at the Nuclear and Energy Research Institute (IPEN-CNEN/SP). Currently, the reactor's fuel elements are composed of low enriched uranium (LEU), i.e., up to < 20% enriched uranium (^{235}U isotope), assembled as fuel plates of U_3Si_2 dispersed in Al. This fuel is manufactured in IPEN's Nuclear Fuel Center, in sequential steps of the nuclear fuel cycle.

During the step of precipitation of uranium tetrafluoride (UF_4), the effluent is collected and subjected to an initial treatment for prior removal of stannous ions (Sn^{2+}) and fluoride ions (F^-), which are present at very high concentrations, about 50 g L^{-1} of Sn and 56 g L^{-1} of F. This previous treatment involves sequential precipitation as $Sn(OH)_4$ and CaF_2, decreasing these species' concentrations in the effluent to acceptable regulatory levels of <4.0 μg L^{-1} for Sn and <10.0 μg L^{-1} for F, according to Brazil's National Council for the Environment, CONAMA (CONAMA, 2011). The first precipitation step is performed by adding Na_2CO_3 to hydrolyze Sn as $Sn(OH)_4$. At this step, part of the uranium is adsorbed on the precipitate because uranium forms a soluble complex with the carbonate. In the second step, CaO is added for F removal as CaF_2 and U, in the form of uranyl fluoride (UO_2F_2), is concomitantly precipitated as calcium diuranate (CaU_2O_7).

Although uranium gets partially removed in this two-step precipitation stage, a remnant concentration of approx. 5 mg L^{-1} of uranium persists in solution, exceeding regulatory levels (CNEN, 2014) and, therefore, it cannot be discharged into the environment as an industrial effluent. The dispersion of radionuclides such as uranium in the aqueous media (surface water and groundwater) can cause serious consequences linked to water consumption. Radionuclides can be taken up and concentrated by aquatic plants and animals, thereby posing a potential risk to animals higher in the food chain, including humans. Also, the radionuclides can deposit in the bottom sediments and concentrate over time, increasing their long term availability to bottom feeders. All of these can have larger implications in particular ecosystems with consequent impacts in biodiversity (IAEA, 2005).

To date, a variety of carbon-based adsorbents has been investigated for U removal from wastewater including activated carbons (Abbasi and Streat, 1994; Kütahyalı and Eral, 2010; Mellah et al., 2006; Öter and Selçuk Zorer, 2019; Saputra et al., 2019) and biochars (Dai et al., 2020; Guilhen et al., 2019a, 2019b; Hadjittofi and Pashalidis, 2015; Zhang et al., 2013; Ding et al., 2018). Previous investigations have demonstrated the efficiency of the non-activated macauba biochar in the removal of uranium (Guilhen et al., 2018; 2019a; 2019b). However, since activated biochars have previously indicated improved sorption capacities, the study of activated macauba biochar for the removal of uranium is justified. To the best of our knowledge, systematic investigations on the effects of physical activation on uranium removal from aqueous solution using macauba endocarp-derived biochar are virtually inexistent in the literature, despite the prevalence of this biomass in tropical regions of the Americas. Macauba is used for production of oil and can also be used for production of biodiesel (Rivera-Utrilla et al., 2011). As a result, large quantities of discarded endocarp accumulate and can pose environmental problems. Identifying an effective use for this material would therefore bring about not only environmental, but also economic benefits (as a result of reduced demand for unsustainable and costly activated carbon). According to our previous investigation (Guilhen et al., 2019b), the low-temperature biochar, namely BC350, was identified as the most promising sorbent among those assessed. Thus, this paper focuses on exploring further improvements that can be achieved by doing the activation of this selected material.

2. Materials and Methods

2.1. Materials

The endocarp from the macauba palm coconut was supplied by SOLEÁ BRASIL (João Pinheiro, MG, Brazil). A standard solution of 1000 mg L^{-1} of uranium was prepared through the dissolution of U_3O_8 certified reference material (CRM 129-A, natural ^{238}U), supplied by New Brunswick Laboratory (New Brunswick, NJ, USA). This solution was used to prepare both adsorption and calibration solutions. All solutions were prepared with ultrapure water (18.2 MΩ cm resistivity) and analytical grade nitric acid (Merck, Darmstadt, HE, Germany).

2.2. Sample preparation

After an initial selection step for the removal of dirt and unbroken coconuts, the clean shells were ground in a cutting mill FA300 (Rone Ind. Com. De Máquinas Ltda., Carapicuíba, SP, Brazil) passing over a 3/8 mesh screen and subsequently air-dried at 100 °C for 3 h.

2.3. Biochar production

A Thermo Fisher Scientific (Asheville, NC, USA), Lindberg Blue M, horizontal tubular steel reactor, with a heating range from 100 to 1100 °C, was used to perform the pyrolysis (Fig. 1). The pyrolysis temperature was set by a central temperature controller and a type K thermocouple was used as secondary control inside the reactor, in the same heating zone where the sample was placed. The samples were placed in an alumina vessel and inserted in the reactor's tube with 0.055 m internal diameter through water-cooled flanges.

Before initiating the pyrolysis, the reactor was purged with argon (Ar) for 20 min. Once the targeted temperature was adjusted, the heating took place under inert argon atmosphere. The carbonized samples were denominated as "BCT", in which "T" corresponds to the highest treatment temperature (HTT); for instance: BC350 is the biochar obtained at the HTT of 350 °C.

Approximately 30 g of dry endocarp was processed at a time, applying an argon gas flow of 40 mL min^{-1} and a 5 °C min^{-1} heating rate. The sample was kept at a specific HTT for 1 h (residence time). Finally, the cooled biochar was ground in a cutting mill passing over a 120 mesh screen.

2.4. Adsorption experiments

Batch technique was used for the equilibrium adsorption experiments, which were performed at room temperature (25 °C) in a rotary shaker MA140 (Marconi Equipamentos para Laboratórios, Piracicaba, SP, Brazil) using 100 mL glass Beckers at 120 rpm stirring rate for 24 h. The adsorbent was separated by filtration using an SCP Science 0.45 μm Teflon membrane filter (Baie-D'Urfé, QC, Canada) and the U(VI) concentration in the reminiscent filtrate solution was determined using a Spectro ARCOS ICP OES (Kleve, NRW, Germany).

The adsorption capacity (mg g^{-1}) of the adsorbent was calculated using Eq. (1):

$$q_t = \frac{(C_0 - C_t) \times V}{M} \quad (1)$$

where "q_t" is the adsorbed amount of adsorbate per gram of

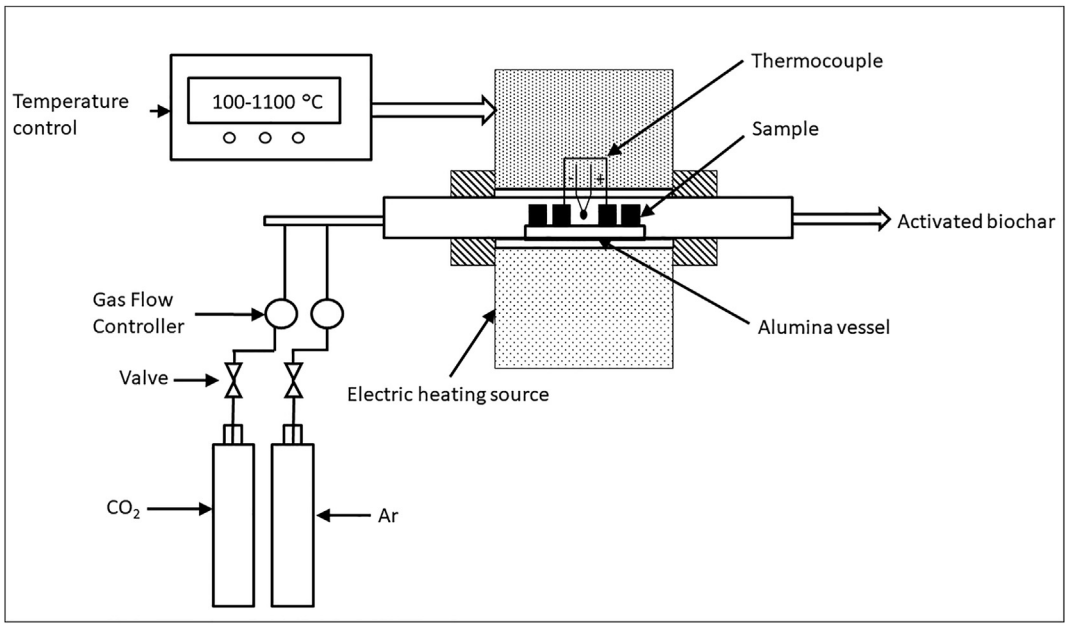

Fig. 1. Scheme of the biochar/activated biochar production apparatus.

adsorbent at any time "t", "C_0" and "C_t" the concentrations of the adsorbate in the initial solution and at any time "t", respectively (mg L^{-1}); "V" the volume of the adsorbate solution added (L) and "M" the amount of the adsorbent used (g).

The extraction efficiency was determined through the following equation (Eq. (2)):

$$R(\%) = \left(\frac{C_o - C_t}{C_o} \right) \times 100 \quad (2)$$

where "R" is the extraction efficiency or retention percentage, "C_0" (mg L^{-1}) is the initial concentration of each adsorbate and "C_t" (mg L^{-1}) represents the concentration of the adsorbate at time "t".

2.4.1. Adsorption using activated BC

Although BC350 performed very promisingly in the removal of uranium from aqueous solutions (Guilhen et al., 2019b), the remaining solution still exceeded regulatory levels (CNEN, 2014). In order to verify if activation enabled the improvement in the adsorption capacity of the macauba biochar, experiments were conducted, comparing both activated (BC350A) and non-activated biochar (BC350), considering various initial uranium concentrations.

To do so, independent duplicates with different U(VI) concentrations, ranging from 1 to 200 mg L^{-1}, were prepared in pH 3 and put in contact with a 10 g L^{-1} dosage of the adsorbents (BC350-A and BC350). The system was subjected to a 120 rpm stirring rate at room temperature for 24 h. These adsorption parameters have been previously established through experimentation and optimized for maximum uranium removal (Guilhen et al., 2019a).

2.5. Physical activation

The process of physical activation, also known as partial degasification (Contescu et al., 2018), was applied to the BC350. When CO_2 is used as activating agent, the activation equation can be described according to the reverse-Boudouard reaction:

$$C + CO_2 \rightleftharpoons 2CO \quad (3)$$

$$\Delta H \cong +170 \text{ kJ mol}^{-1} \text{ at } 298 \text{ K}.$$

The reaction is endothermic, i.e., the product is higher in energy than the reactants. Therefore, the change in enthalpy is positive and heat must be supplied to favor the reaction. Temperatures above 700 °C are required to promote the reaction.

The activation was carried out by heating the BC350 up until 850 °C under Ar atmosphere at a 10 °C min^{-1} heating rate. Once the sample reached 850 °C, the Ar supply was interrupted and a 20 mL min^{-1} flow of CO_2 was introduced in the pyrolysis reactor (Castro, 2009), replacing the Ar flow. The sample was kept under these conditions for 2 h.

After activation, the sample was acid washed using 0.5 mol L^{-1} of HCl to remove impurities from inside the pores, followed by subsequent washes with warm and cool distilled water. The activated sample, denominated "BC350-A", was oven-dried at 110 °C and stored in a desiccator before further use.

2.6. N_2 adsorption analysis

The N_2 adsorption analysis at 77 K was performed using Micromeritics, TriStar II 3020 V1.03 (Norcross, GA, USA), surface, and porosity analyzer.

2.7. Adsorption isotherm models

Four isotherm models (Langmuir, Freundlich, Toth and Redlich-Peterson) were tested for modeling the adsorption isotherms by nonlinear method. See the supplementary material for further details on the isotherm models.

2.8. Parameter estimation

A "search method" called *Downhill Simplex* was used to optimize the parameters in order to adjust the mathematical models that most accurately represent the observed date. See the

supplementary material for a full description of the method.

2.9. Characterization

Nitrogen adsorption analysis was used to characterize the biochar's specific surface area and adsorption isotherms were obtained to assess the U(VI) adsorption onto the activated biochar. Surface analysis was evaluated by Fourier-Transform infrared spectroscopy (FTIR), the morphology of the activated and non-activated biochars was observed by scanning electron microscopy (SEM) analysis and the presence of U(VI) was detected by micro X-ray fluorescence spectrometry.

Surface analysis was carried out using a PerkinElmer Spectrum One FTIR spectrophotometer (PerkinElmer Inc., Waltham, USA). High-resolution imaging of both activated and non-activated biochars were obtained using a FEI Quanta 650FEG scanning electron microscope (FEI Company, Hillsboro, USA). A Shimadzu Micro X-ray fluorescence spectrometer μ-EDX 1300 (Shimadzu Corporation, Kyoto, Japan) was used to confirm the presence of uranium in the activated biochar. A Spectro ARCOS inductively coupled plasma optical emission spectrometer (Spectro Analytical Instruments Co., Kleve, Germany) and a Thermo iCAP inductively coupled plasma mass spectrometer (Thermo Fisher Scientific, Waltham, USA) were employed for multi-element analysis.

2.10. Application in treatment of U(VI) effluent

A multi-elemental analysis of the residual effluent, previously treated to remove Sn and F, was performed in order to determine which other elements were present in such amounts that could interfere or compete in the process of U(VI) adsorption. Also, the residual effluent is alkaline (pH approx. 8) and a previous study with BC350 showed that a better performance was achieved when U(VI) solution was adjusted to pH 3 (Guilhen et al., 2019a). The adsorption parameters have been optimized using the biochar obtained at 350 °C (BC350), because it was the temperature at which the gravimetric yield factor provided the best compromise between fixed carbon and gravimetric yield (Guilhen et al., 2019b).

The removal of U(VI) from the aqueous pre-treated UF_4 effluent using BC350-A was evaluated by testing three sub-samples, with solution pH values adjusted from 8 to 3 before addition of the adsorbent (Guilhen et al., 2019a). Inductively coupled plasma mass spectrometry (ICP-MS) was used for the determination of the remaining U(VI) in solution.

3. Results and discussion

3.1. Activation

Uranium adsorption onto BC350-A was evaluated for a wide range of solution concentrations between 1 and 200 mg L^{-1}, adjusted to pH 3, using an adsorbent dosage of 10 g L^{-1}. The results are shown in Fig. 2.

The uranium removal was significantly higher on the activated biochar (BC350-A), achieving over 99% removal for an initial concentration of 5 mg L^{-1}, whereas for the non-activated biochar (BC350), the removal efficiency achieved was of 80.5% at the same initial concentration (Guilhen et al., 2019b). The average remaining concentration of U(VI) was 0.041 mg L^{-1} (41 μg L^{-1}) and the final pH measured was 5.7. Additionally, the removal efficiency was over 90% and practically constant for a wider range of concentrations (2.5–25 mg L^{-1}) when the activated BC was used.

The adsorption capacity (q) of BC350-A increased with increasing initial uranium concentrations. At an initial uranium concentration of 5 mg L^{-1}, the adsorption capacity was 422.0 mg g^{-1} for BC350 (Guilhen et al., 2019b) and 488.7 mg g^{-1} for BC350-A (Table S3). The highest uranium adsorption capacity (q = 11,750 mg g^{-1}) in the range investigated was achieved at an initial concentration of 200 mg L^{-1} when BC350-A was used.

The BC350-A behavior can be explained in terms of exchangeable sites in the activated adsorbent structure, evidencing that the activation process successfully increased the adsorption sites in the biochar structure. According to Gulnaz et al. (2004), the initial increase in the adsorbate's concentration will increase the driving force of the concentration gradient, causing an increase in adsorption capacity.

As the ratio of uranium to BC350-A ($[U]/m_{BC350\text{-}A}$) increases, the exchangeable sites in the BC structure get saturated, resulting in decreasing driving force and removal efficiency. In contrast, the adsorption capacity increased with initial uranium concentration (constant mass of adsorbent), which may be due to an increase in the driving force of the concentration gradient as the initial adsorbate concentration increased.

The adsorption capacity achieved for an initial uranium concentration of 5 mg L^{-1} (q_e = 488.7 mg g^{-1}) was used to compare the efficiency of BC350-A with other materials, which have been previously tested as adsorbents for U(VI). When compared to other organic, inorganic and biological adsorbents reported in literature, BC350-A is among the highest performing adsorbents for U(VI) adsorption (Table S1).

3.2. N_2 adsorption analysis

N_2 adsorption analysis allowed the determination of the specific surface area (BET), pore volume and mean pore size for the activated and non-activated biochar samples, BC350-A and BC350, respectively. The results obtained are presented in Table S2.

As expected, the BET surface area increased with activation. Biochar activation took place at 850 °C, 500° higher than the pyrolytic temperature employed to produce the BC350 sample. Surface area increased with increasing temperatures due to the escape of volatile substances and the formation of channels in the biochar structure. The porosity development is further promoted by the gasification process during physical activation with CO_2. The activation results are consistent with what has been described in the literature (Ahmad et al., 2012; Chen et al., 2012; Kim et al., 2013).

The N_2 adsorption-desorption isotherm for BC350 and BC350-A are shown in Fig. S1. Type II-isotherm best fits the BC350, according to the IUPAC's classification (Martín-Martínez, 1990; Thommes et al., 2015). Type II isotherms are observed for nonporous or macroporous materials.

Generally, isotherms obtained for physically activated charcoals tend to correspond to the Type IV, traditionally attributed to mesoporous solids with a significant microporous fraction (Crini and Badot, 2011). However, the isotherm obtained for BC350-A is compatible with Type I isotherms, according to the IUPAC's classification (Thommes et al., 2015), which represent microporous solids.

Type I isotherms show a rapid increase in adsorbed gas pressure as pressure increases until reaching a plateau. This is due to the great ease of adsorption in pores with diameters smaller than 2 nm. After micropore filling, there are virtually no other regions where adsorption is significant. The curve, therefore, exhibits an almost constant region and grows back when condensation begins to take place (Teixeira et al., 2001).

The isotherm shown in Fig. S1 (BC350-A) exhibits a hysteresis cycle. The upward curve represents the measurements obtained by progressive addition of the adsorbent gas (adsorption) until saturation, while the downward curve represents the progressive withdrawal (desorption) (Rouquerol et al., 1999). According to the

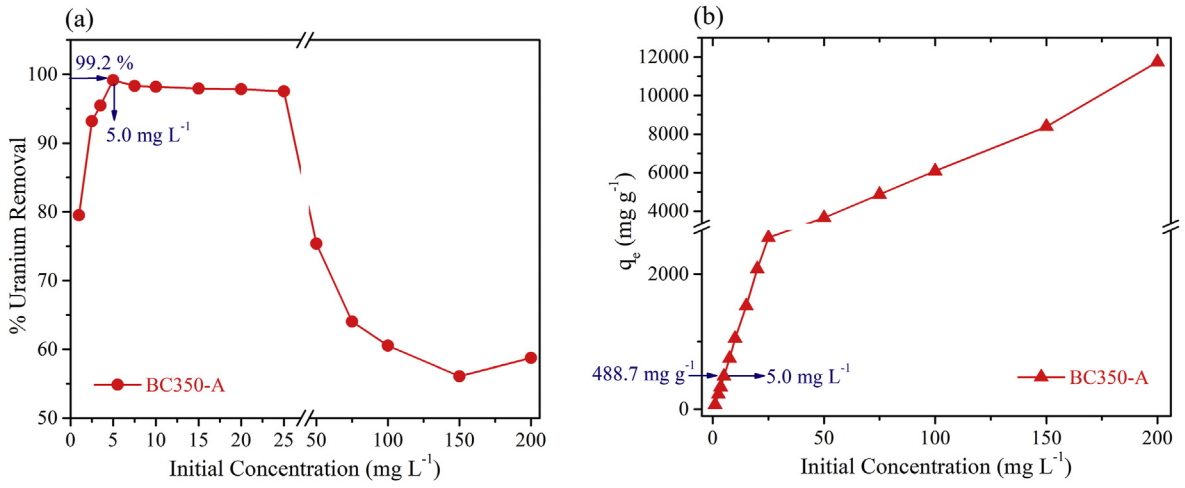

Fig. 2. Removal efficiency (a) and adsorption capacity (b) for BC350-A.

IUPAC's classification (Martín-Martínez, 1990), this cycle has the aspect of "H4", being associated with narrow slit pores with wedge shapes, cones and/or parallel plates and cylindrical capillaries open at both ends (Lowell et al., 2012; Sing, 1985; Thommes, 2010; Thommes et al., 2013, 2015).

It is also observed that for low relative pressure values ($P/P_0 \approx 0.1$), the volume of N_2 adsorbed by BC350-A is 3×10^{-1} cm^3 g^{-1}, which is much higher compared to the volume adsorbed by BC350 (1.4×10^{-3} cm^3 g^{-1}). This increase in adsorbed volume at low relative pressures is due to a higher microporous development (<2 nm), which leads to a larger specific surface area in the BC350-A. When $P/P_0 \approx 1$, the volume of adsorbed gas is also higher for the activated sample and, in this case, this is related to the maximum capacity of total gas adsorption by the solid, evidencing the highest porosity in the activated biochar.

Pore size distribution for BC350 is shown in Fig. S2. A predominance of medium-sized porous, characteristic of mesoporous materials (2–50 nm), with an average pore size of 30 nm was observed. However, a significant macroporous fraction (>50 nm) was observed, which is consistent to the surface area of 0.83 m^2 g^{-1} (0.5–2 m^2 g^{-1}) as shown in Table S2.

Pore size distribution for BC350-A is shown in Fig. S2. A prevalence of micropores can be observed as a consequence of the physical activation, contributing to the increase of micropore volume (Table S2). The average pore size of BC350-A was 2.9 nm and the pore volume was 0.3 cm^3 g^{-1}, characterizing the activated material as essentially microporous. Therefore, the isotherm data were adjusted by the t-plot method.

Comparison of the porous structure of activated and non-activated samples indicates that the activation process clearly led to an increase in porosity of activated samples. The porosity (P) of BC350-A was determined as the volume of voids in the biochar, calculated according to Eq. (4):

$$P(\%) = \frac{(True\ density - Bulk\ density) \times 100\%}{True\ density} \quad (4)$$

BC350-A's true (1.98 g cm^{-3}) and bulk densities (0.74 g cm^{-3}) were applied in Eq. (4) and the calculated porosity (P) is approximately 63%. Therefore, BC350-A can be classified as a material of very high porosity (P > 50%) (Fiori and Carmignani, 2001).

3.3. Adsorption isotherms

The results of the U adsorption on the activated biochar, BC350-A, are presented in Table S3 and could be mathematically represented by isotherms. Langmuir, Freundlich, Toth and Redlich-Peterson isotherms were employed in the study of the U/BC350-A system. The obtained graphs are shown in Fig. 3.

The respective parameters, obtained by non-linear regression for each isotherm model, are shown in Table 1.

The highest degree of correlation, using Pearson's correlation coefficient (R^2), was obtained for Freundlich and Redlich-Peterson adsorption isotherms at 0.93 and 0.95, respectively, compared to Langmuir and Toth adsorption isotherms (0.88 and 0.87, respectively).

However, the R^2 values for Freundlich and Redlich-Peterson are very close to each other, making it difficult to use this parameter as a selection criterion. Thus, an estimate of the best fit for the isotherm model was performed by calculating different equations for deviation estimate, also called "error functions" (Foo and Hameed, 2010) as shown in Table S4.

Since mathematical models are only an attempt to describe reality (Ncibi, 2008), the deviation estimates are better suited to obtain a more accurate fit. The deviation estimates, shown in Table S4, compare the experimental q_e (q_{eexp}), described in Table S3,

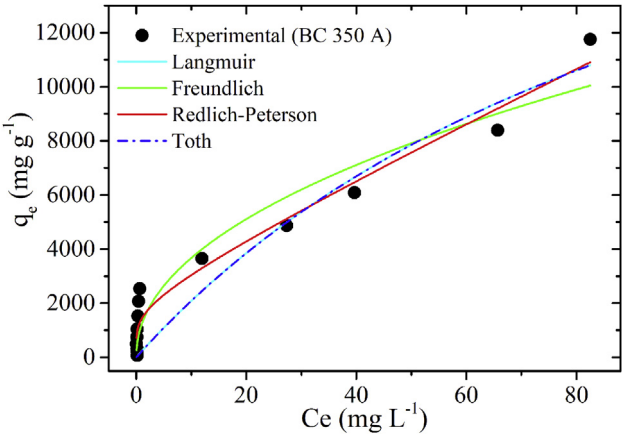

Fig. 3. Adsorption isotherms of the U onto BC350-A.

Table 1
Experimental parameters of the adsorption isotherm models of the U/BC350-A system.

Isotherms	Parameters			
Langmuir	Q_{max}(mg g^{-1})	K_L(L mg^{-1})		$R^2_{adj.}$
	107.08	2.12		0.883
Freundlich	K_F((mg g^{-1}) (mg $L^{-1})^{-1/nF}$)	n_F		$R^2_{adj.}$
	69.94	2.09		0.927
Toth	K_T (L mg^{-1})	a_T(L mg^{-1})	t	$R^2_{adj.}$
	2.22	0.47	0.02	0.872
R-P	K_{RP} (L g^{-1})	a_{RP}(mg $L^{-1})^{-\beta}$	β	$R^2_{adj.}$
	93.59	16.48	0.19	0.955

with the calculated q_e (q_{ecalc}) using the equations shown in Table S4. The lower values of these estimates indicate the best fitting isotherms.

The most suitable model for satisfactorily describing the adsorption phenomenon of the U/BC350-A system is based on the highest determination coefficient (R^2) and the lowest values of RAE, SSR, MPSD, HYBRID, SAE and X^2 altogether.

As can be seen in Table S5, the Redlich-Peterson model provided the best fit of the experimental data, suggesting heterogeneity of adsorption sites (Olivelli et al., 2013), with different affinities for uranium, or the existence of a cooperative effect (Hinz, 2001), which increases the affinity between uranyl ions and adsorption sites.

Since the Redlich-Peterson equation is a hybrid isotherm, that incorporates functionalities of both the Langmuir and the Freundlich isotherms (Foo and Hameed, 2010), it was expected that the fit of the experimental data for this equation would be better than that obtained with the Langmuir and Freundlich equations. The modeling reveals, thus, a hybrid adsorption mechanism.

This supports previous findings in recent literature. For instance, Li et al. (2019) employed biochar derived from *Ficus microcarpa* aerial root and also compared raw and modified biochar. Their findings also indicated the Redlich-Peterson to be the best fitting isotherm for both biochars ($R^2 = 0.96$ for raw biochar, $R^2 = 0.98$ for modified biochar). Another example is the work of Vieira et al. (2019), who studied the adsorption of U(VI) onto macrophytes. For *Pistia stratiotes*, the Redlich-Peterson equation provided the best fit for the experimental data ($R^2 = 0.86$, corrected Akaike information criterion = −175.2).

3.4. Characterization

A comparison of FTIR spectra of BC350 and BC350-A is shown in Fig. 4. The FTIR spectra for BC350 have been already discussed in a previous study (Guilhen et al., 2019b) and Fig. 4 contrasts it against that of activated biochar.

The absorption bands attributed to the OH stretching of hydroxyl and carboxylic acid groups (3600−3300 cm^{-1}) and to the C=C stretching of aromatic structures (1650−1520 cm^{-1}), that are practically non-existent in the BC350-A spectrum, are much more pronounced in the BC350 spectrum. Previous findings (Guilhen et al., 2019b) showed that the uranyl ions were adsorbed onto BC350 by chemisorption, enabled by hydroxyl and carboxylic acid surface groups. Other bands corresponding to the $-CH_2$ and $-CH_3$ stretching of aliphatic chains (2942 cm^{-1}) and aromatic −CO and phenolic −OH at 1270 cm^{-1} were also considerably reduced in the BC350-A sample.

These spectra are in agreement with previous observations (Guilhen et al., 2019b) and are the result of the process of thermal decomposition, in which the increase in the pyrolytic temperature causes loss of surface functional groups and subsequent decrease in acidity and polarity of the surface (Kim et al., 2013), indicating that physisorption is the ruling mechanism of adsorption in the U/BC350-A system and was enabled because of the increased specific surface area of the BC350-A.

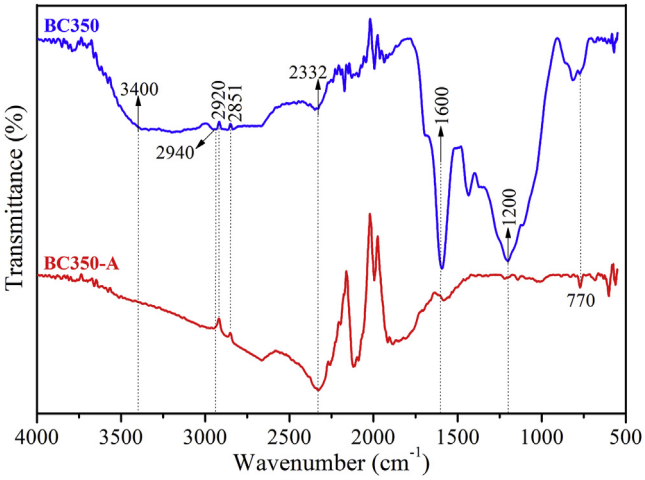

Fig. 4. FTIR/UATR vibrational spectrum of BC350 and BC350-A.

The micrographs shown in Figs. 5 and 6 correspond to the topography images of the BC350 and BC350-A, respectively.

Despite the high heterogeneity of the surfaces, the morphology of BC350 is very characteristic of chars, with porous cavities and intertwined channels formed by the transport of water vapor and volatiles to the surface of the material (Bandosz, 2006).

In the micrographs of BC350-A (shown in Fig. 6) it is possible to observe a morphology that is characteristic of activated chars. The release of volatile components promoted the formation of a structure with vascular bundles or channels that provide greater permeability to the material due to the increased surface area.

These microscopic images evidence the role of activation in removing residues that remained from the biomass decomposition and the volatilization of bituminous substances and tars during the process of carbonization, in which rudimentary pores are already created. On physical activation, these residues react with the flow of gases (in this case, CO_2) at elevated temperatures (850 °C), getting oxidized. As a result, the pre-existing pores get cleared and widened (because CO_2 oxidizes the carbonaceous material present inside the pores as well), increasing the surface area. An increased surface area exposes more surface groups, favoring chemical and physical interactions with uranyl ions.

Energy-dispersive micro X-ray fluorescence spectrometry (Micro-XRF) was employed to detect the presence of adsorbed uranium in BC350-A. This technique was selected over the conventional XRF because of its sensitivity, capable of detecting uranium in lower concentrations. Therefore, this technique provides evidence that the uranium was actually absorbed onto BC350-A. The results are shown in Table S6.

The characteristic X-rays emitted by the innermost layers of a given element are grouped under the name K_α and K_β, resulting from electronic transitions L → K and M → K, respectively (Lyman series). Similarly, the characteristic X-ray emission lines L_α and L_β originate from the electronic transition of the layers M → L ($L_{\alpha1}$, $L_{\alpha2}$ e $L_{\beta1}$) and N → L ($L_{\beta2}$) (Balmer series) (Khoury Asfora, 2010).

The emission line K_α characteristic of "Fe" has a very low intensity, indicating its presence as a probable impurity in the material. The K_α and $K_{\alpha C}$ (Compton) lines of Rh are due to the Rh tube (the X-ray source).

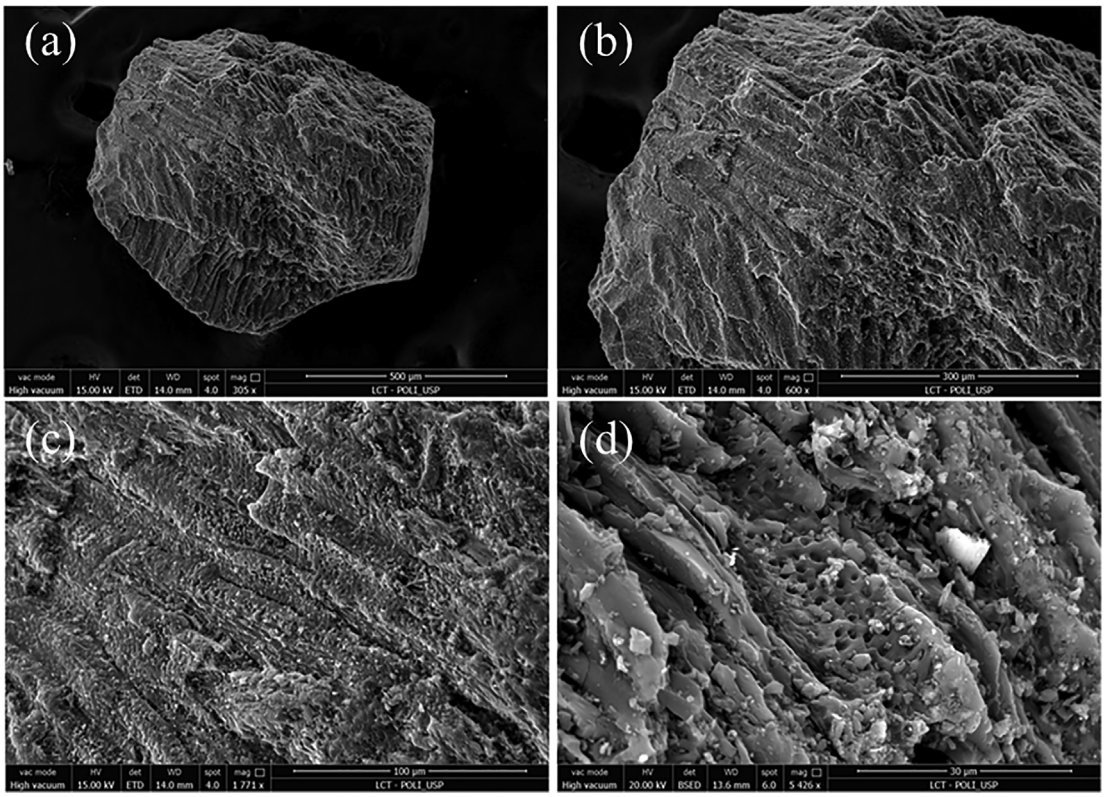

Fig. 5. BC350 micrographs obtained by SEM in different magnifications: (a) 305x; (b) 600x; (c) 1,771x; (d) 5,426x.

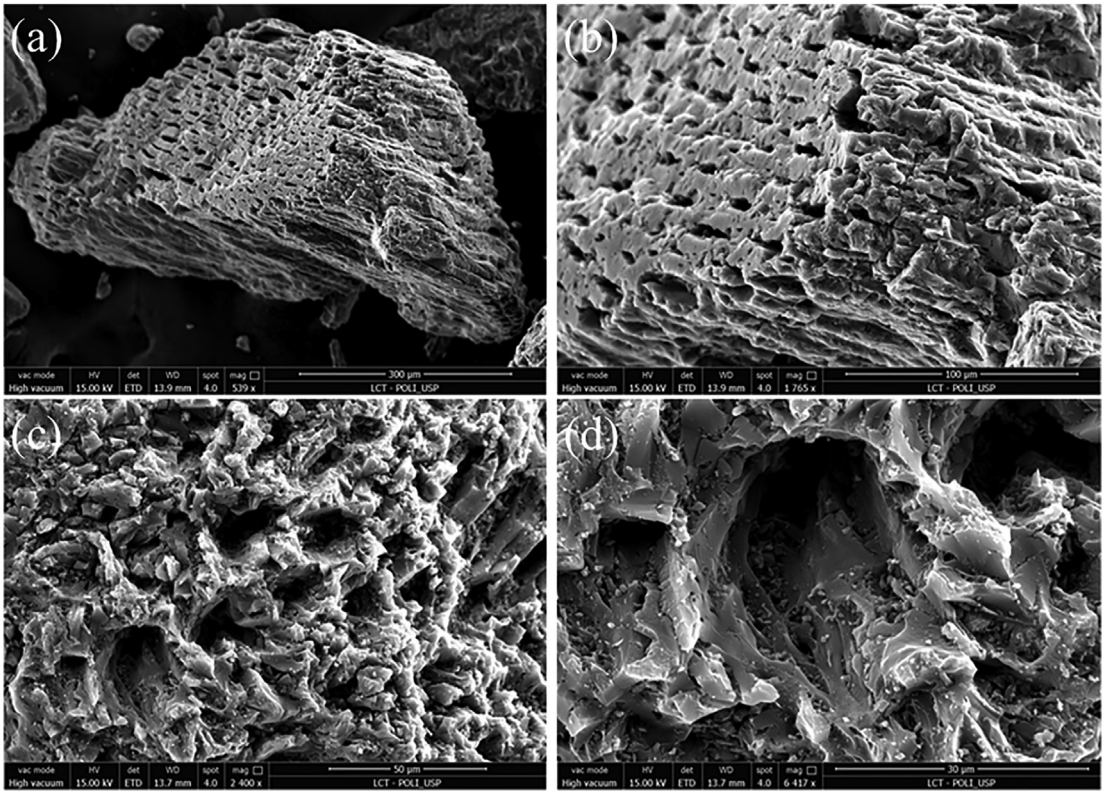

Fig. 6. BC350-A micrographs obtained by SEM in different magnifications: (a) 539x; (b) 1,765x; (c) 2,400x; (d) 6,417x.

Table 2
Sn, U and F levels after the pre-treatment in the Nuclear Fuel Center.

Element ($\mu g\ mL^{-1}$)	Effluent (Initial)	Effluent (Final)	Maximum levels	Regulatory Agency
Sn	$5 \times 10^4 \pm 1.6 \times 10^2$	< LOD	4	CONAMA (2011)
U	$7.6 \times 10^1 \pm 3 \times 10^{-1}$	5.1 ± 0.6	2.2×10^{-1}	CNEN (2014)
F	$5.6 \times 10^4 \pm 1.4 \times 10^2$	5.7 ± 0.5	10	CONAMA (2011)

*LOD = 0.5 $\mu g\ mL^{-1}$

Exposure of the sample to the X-ray beam promotes the excitation of the L layers in the adsorbed U. The β transition lines of U (16.48 keV and 17.23 keV) are the least likely to occur and have higher energy than the α transition line (13.66 keV). The indices "1" and "2" in the transitions $L_{\beta 1}$ and $L_{\beta 2}$ indicate the transition between the sublayers M-IV → L-II and N–V → L-III. The most intense transition occurs in L_{α}. Since uranium has electrons distributed in layers of orders higher than M, it is also possible to identify a transition U M_{β} referring to the transition N–V (O) → N-3 (M) (Paschen series).

Micro-XRF analysis provided an efficient way to identify the U present in the adsorbent, thus proving the effective adsorption onto BC350-A.

3.5. Application in UF_4 effluent treatment

As can be seen in Table 2, the sequential initial treatment reduced the concentration of Sn and F species in solution to values lower than the allowable limits according to the Resolution nº 430 of the Brazilian National Council for the Environment, CONAMA (CONAMA, 2011).

However, CONAMA's Resolution Nº 430 (CONAMA, 2011) does not include the maximum values for U release. Therefore, the liberation of effluents containing U must comply with CNEN's resolution CNEN–NN–8.01 (CNEN, 2014), for which the maximum limit for the mixture of U isotopes in the UF_4 effluent (80.25% for ^{238}U and 19.75% ^{235}U isotopic ratio) was calculated according to their respective specific activities, considering an allowable discharge level of 5.6 kBq m^{-3} for both isotopes (see section 3.5 of the supplementary Material).

According to the results presented in Table 2, the two-step treatment resulted in a solution in which the remaining U concentration was 5 mg L^{-1}, therefore, not efficient enough to comply with the regulatory demands (CNEN, 2014).

A complementary treatment of this solution, initially at pH 8, was performed using the activated biochar (BC350-A) and the pH of the solution was adjusted to 3. After adsorption, the remaining U concentration in solution was 1.1×10^{-1} $\mu g\ mL^{-1}$ (2.8 kBq m^{-3}). The presence of Na^+ ions in the solution (2.7×10^3 $\mu g\ mL^{-1}$) has likely influenced the adsorption process, decreasing the removal efficiency initially achieved for the aqueous solution (Na^+ free) from 99.2% (4.1×10^{-2} $\mu g\ mL^{-1}$) to 97.9% (1.1×10^{-1} $\mu g\ mL^{-1}$). Other elements such as Mg, B, Zn, Ni, As, Cu, Ba, Cr, Pb, Mn, Se, Fe, Cd and Ag were also determined in the UF_4 effluent by ICP OES, but none of them scored higher than 1×10^{-1} $\mu g\ mL^{-1}$, therefore, their influence were considered negligible regarding coexistence interactions. Moreover, the U concentration in the treated solution was below the maximum allowable limits of 5.6 kBq m^{-3} (CNEN, 2014).

4. Conclusion

CO_2 physical activation significantly enhanced the adsorption capacity of macauba endocarp-derived biochar for uranyl ions in aqueous solutions, achieving over 99% removal for an initial concentration of 5 mg L^{-1}. The activation process led to an increase in porosity with a specific surface area increasing from 0.83 to 643 $m^2\ g^{-1}$. Chemical surface of the biochar was significantly affected by activation. According to the FTIR analysis, the activation process increased the aromaticity of the biochar, indicating that the uranium adsorption was carried out by physical interactions. The adsorption of uranyl ions onto the activated biochar was confirmed by μ-EDX analysis. The Redlich-Peterson three-parameter equation isotherm model was the most appropriate for fitting the experimental data, suggesting heterogeneity of adsorption sites with different affinities for uranium setting up as a hybrid adsorption mechanism. Finally, treating an actual U-containing effluent with BC350-A has proven to be efficient in meeting the regulatory requirements. This study has therefore shown that an ubiquitous low-cost biomass material such as macauba palm endocarp can be successfully converted to activated biochar and used in treatment of industrial effluents, specifically those containing uranyl ions.

Declaration of competing interest

The authors declare that they have no known competing financial interests or personal relationships that could have appeared to influence the work reported in this paper.

Acknowledgements

The authors would like to thank Mr. Felipe Morbi, CEO of SOLEÁ BRASIL (João Pinheiro, Brazil), for supplying the macauba endocarp, and the Brazilian National Nuclear Energy Commission (CNEN), for supporting this study.

Appendix A. Supplementary data

Supplementary data to this article can be found online at https://doi.org/10.1016/j.envpol.2020.116022.

References

Abbasi, W.A., Streat, M., 1994. Adsorption of uranium from aqueous solutions using activated carbon. Separ. Sci. Technol. 29, 1217–1230.
Ahmad, M., Lee, S.S., Dou, X., Mohan, D., Sung, J.-K., Yang, J.E., Ok, Y.S., 2012. Effects of pyrolysis temperature on soybean stover-and peanut shell-derived biochar properties and TCE adsorption in water. Bioresour. Technol. 118, 536–544.
Bandosz, T.J., 2006. Activated Carbon Surfaces in Environmental Remediation. Elsevier.
Bansal, R.C., Goyal, M., 2005. Activated carbon adsorption. CRC press.
Castro, C.S., 2009. Preparação de carvão ativado a partir de borra de café: uso como adsorvente e como suporte catalítico para a remoção de poluentes orgânicos em meio aquoso.
Chen, X., Chen, G., Chen, L., Chen, Y., Lehmann, J., McBride, M.B., Hay, A.G., 2011. Adsorption of copper and zinc by biochars produced from pyrolysis of hardwood and corn straw in aqueous solution. Bioresour. Technol. 102, 8877–8884.
Chen, Z., Chen, B., Zhou, D., Chen, W., 2012. Bisolute sorption and thermodynamic behavior of organic pollutants to biomass-derived biochars at two pyrolytic temperatures. Environ. Sci. Technol. 46, 12476–12483.
Claudino, A., 2003. Preparação de carvão ativado a partir de turfa e sua utilização na remoção de poluentes.
Cnen, 2014. Norma CNEN NN 8.01 resolução CNEN 167/14 abril/2014. Gerência de rejeitos radioativos de baixo e médio níveis de radiação - Resolução CNEN Nº 167/14 44.
CONAMA, 2011. Condições, parâmetros, padrões e diretrizes de gestão do lançamento de efluentes em corpos de água receptores (Brazil).
Contescu, C.I., Adhikari, S.P., Gallego, N.C., Evans, N.D., Biss, B.E., 2018. Activated carbons derived from high-temperature pyrolysis of lignocellulosic biomass. C—Journal Carbon Res. 4, 51.
Crini, G., Badot, P.-M., 2011. Sorption Processes and Pollution: Conventional and Non-conventional Sorbents for Pollutant Removal from Wastemasters. Presses Univ. Franche-Comté.
Dai, L., Li, L., Zhu, W., Ma, H., Huang, H., Lu, Q., Yang, M., Ran, Y., 2020. Post-engineering of biochar via thermal air treatment for highly efficient promotion of uranium (VI) adsorption. Bioresour. Technol. 298, 122576.
Dalai, A.K., Azargohar, R., 2007. Production of activated carbon from biochar using chemical and physical activation: mechanism and modeling. ACS Publications.

De Celis, J., Amadeo, N.E., Cukierman, A.L., 2009. In situ modification of activated carbons developed from a native invasive wood on removal of trace toxic metals from wastewater. J. Hazard Mater. 161, 217–223.
Ding, L., Tan, W.-F., Xie, S.-B., Mumford, K., Lv, J.-W., Wang, H.-Q., Fang, Q., Zhang, X.-W., Wu, X.-Y., Li, M., 2018. Uranium adsorption and subsequent Re-oxidation under aerobic conditions by leifsonia sp. – coated biochar as green trapping agent. Environ. Pollut 242, 778–787.
Feng, D., Zhang, Y., Zhao, Y., Sun, S., Gao, J., 2018. Improvement and maintenance of biochar catalytic activity for in-situ biomass tar reforming during pyrolysis and H2O/CO2 gasification. Fuel Process. Technol. 172, 106–114.
Fiori, A.P., Carmignani, L., 2001. Fundamentos de mecânica de solos e das rochas: aplicações na estabilidade de taludes. Editora da UFPR.
Foo, K.Y., Hameed, B.H., 2010. Insights into the modeling of adsorption isotherm systems. Chem. Eng. J. 156, 2–10.
Franciski, M.A., Peres, E.C., Godinho, M., Perondi, D., Foletto, E.L., Collazo, G.C., Dotto, G.L., 2018. Development of CO_2 activated biochar from solid wastes of a beet industry and its application for methylene blue adsorption. Waste Manag. 78, 630–638.
Gorgulho, H.F., Mesquita, J.P., Gonçalves, F., Pereira, M.F.R., Figueiredo, J.L., 2008. Characterization of the surface chemistry of carbon materials by potentiometric titrations and temperature-programmed desorption. Carbon N. Y. 46, 1544–1555.
Grand View Research, 2019. Activated carbon market size, share & trends analysis report 2019-2025 [WWW document]. https://www.grandviewresearch.com/industry-analysis/activated-carbon-market.
Guilhen, S.N., Rovani, S., Pitol Filho, L., Alves Fungaro, D., 2018. Kinetic study of uranium removal from aqueous solutions by macaúba biochar. Chem. Eng. Commun. 206, 1365–1377.
Guilhen, S.N., Coleti, J., Tenório, J.A.S., Fungaro, D.A., 2019a. Influence of pyrolytic temperature on uranium adsorption capability by biochar derived from macauba coconut residue. Brazilian J. Radiat. Sci. 7.
Guilhen, S.N., Mašek, O., Ortiz, N., Izidoro, J.C., Fungaro, D.A., 2019b. Pyrolytic temperature evaluation of macauba biochar for uranium adsorption from aqueous solutions. Biomass Bioenergy 122, 381–390.
Gulnaz, O., Kaya, A., Matyar, F., Arikan, B., 2004. Sorption of basic dyes from aqueous solution by activated sludge. J. Hazard Mater. 108, 183–188.
Hadjittofi, L., Pashalidis, I., 2015. Uranium sorption from aqueous solutions by activated biochar fibres investigated by FTIR spectroscopy and batch experiments. J. Radioanal. Nucl. Chem. 304, 897–904.
Hinz, C., 2001. Description of sorption data with isotherm equations. Geoderma 99, 225–243.
IAEA – International Atomic Energy Agency, 2005. Environmental contamination from uranium production facilities and their remediation. In: Proceedings of an International Workshop, Lisbon, 11–13 February 2004.
Kalderis, D., Bethanis, S., Paraskeva, P., Diamadopoulos, E., 2008. Production of activated carbon from bagasse and rice husk by a single-stage chemical activation method at low retention times. Bioresour. Technol. 99, 6809–6816.
Khoury Asfora, V., 2010. Fluorescência de Raios X por dispersão de energia aplicada à caracterização de tijolos de sítios históricos de Pernambuco.
Kim, W.-K., Shim, T., Kim, Y.-S., Hyun, S., Ryu, C., Park, Y.-K., Jung, J., 2013. Characterization of cadmium removal from aqueous solution by biochar produced from a giant Miscanthus at different pyrolytic temperatures. Bioresour. Technol. 138, 266–270.
Kütahyalı, C., Eral, M., 2010. Sorption studies of uranium and thorium on activated carbon prepared from olive stones: kinetic and thermodynamic aspects. J. Nucl. Mater. 396, 251–256.
Kwiatkowski, J.F., 2011. Activated Carbon: Classifications, Properties and Applications. Nova Science Publishers (Incorporated).
Le Cloirec, P., Faur-Brasquet, C., 2008. Adsorption of inorganic species from aqueous solutions. In: Adsorption by Carbons. Elsevier, pp. 631–651.
Li, N., Yin, M., Tsang, D.C.W., Yang, S., Liu, J., Li, X., Song, G., Wang, J., 2019. Mechanisms of U(VI) removal by biochar derived from Ficus microcarpa aerial root: a comparison between raw and modified biochar. Sci. Total Environ. 697, 134115.
Lowell, S., Shields, J.E., Thomas, M.A., Thommes, M., 2012. Characterization of porous solids and powders: surface area, pore size and density. Springer Science & Business Media.
Maciá-Agulló, J.A., Moore, B.C., Cazorla-Amorós, D., Linares-Solano, A., 2004. Activation of coal tar pitch carbon fibres: physical activation vs. chemical activation. Carbon N. Y. 42, 1367–1370.
Marsh, H., Reinoso, F.R., 2006. Activated Carbon. Elsevier.
Martín-Martínez, J.M., 1990. Adsorción física de gases y vapores por carbones. Universidad de Alicante, Secretariado de Publicaciones.
Mellah, A., Chegrouche, S., Barkat, M., 2006. The removal of uranium (VI) from aqueous solutions onto activated carbon: kinetic and thermodynamic investigations. J. Colloid Interface Sci. 296, 434–441.
Mestre, A.S., Carvalho, A.P., 2018. Nanoporous carbons synthesis: an old story with exciting new chapters. In: Porosity, Ghrib, T. (Eds.), IntechOpen London, UK, pp. 37–68.
Mezohegyi, G., van der Zee, F.P., Font, J., Fortuny, A., Fabregat, A., 2012. Towards advanced aqueous dye removal processes: a short review on the versatile role of activated carbon. J. Environ. Manag. 102, 148–164.
Molina-Sabio, M., Gonzalez, M.T., Rodriguez-Reinoso, F., Sepúlveda-Escribano, A., 1996. Effect of steam and carbon dioxide activation in the micropore size distribution of activated carbon. Carbon N. Y. 34, 505–509.
Ncibi, M.C., 2008. Applicability of some statistical tools to predict optimum adsorption isotherm after linear and non-linear regression analysis. J. Hazard Mater. 153, 207–212.
Nunell, G.V., Fernández, M.E., Bonelli, P.R., Cukierman, A.L., 2012. Conversion of biomass from an invasive species into activated carbons for removal of nitrate from wastewater. Biomass Bioenergy 44, 87–95.
Olivelli, M.S., Curutchet, G.A., Torres Sánchez, R.M., 2013. Uranium uptake by montmorillonite-biomass complexes. Ind. Eng. Chem. Res. 52, 2273–2279.
Öter, Ç., Selçuk Zorer, Ö., 2019. Adsorption behaviours of Th (IV) and U(VI) using nitric acid (HNO3) modified activated carbon: equilibrium, thermodynamic and kinetic studies. Int. J. Environ. Anal. Chem 1–16.
Peng, H., Gao, P., Chu, G., Pan, B., Peng, J., Sing, B., 2017. Enhanced adsorption of Cu (II) and Cd (II) by phosphoric acid-modified biochars. Environ. Pollut. 229, 846–853.
Rajapaksha, A.U., Vithanage, M., Ahmad, M., Seo, D.-C., Cho, J.-S., Lee, S.-E., Lee, S.-S., Ok, Y.S., 2015. Enhanced sulfamethazine removal by steam-activated invasive plant-derived biochar. J. Hazard Mater. 290, 43–50.
Ramanujan, R.V., Purushotham, S., Chia, M.H., 2007. Processing and characterization of activated carbon coated magnetic particles for biomedical applications. Mater. Sci. Eng. C 27, 659–664.
Rivera-Utrilla, J., Sánchez-Polo, M., Gómez-Serrano, V., Alvarez, P.M., Alvim-Ferraz, M.C.M., Dias, J.M., 2011. Activated carbon modifications to enhance its water treatment applications. An overview. J. Hazard Mater. 187, 1–23.
Rocha, W.D., Luz, da, Lena, J.A.M. da, de, J.C., Bruña-Romero, O., 2006. Adsorção de cobre por carvões ativados de endocarpo de noz macadâmia e de semente de goiaba. Rem 59, 409–414.
Rodriguez-Reinoso, F., Silvestre-Albero, J., 2016. Activated carbon and adsorption.
Roman, S., Nabais, J.M.V., Ledesma, B., González, J.F., Laginhas, C., Titirici, M.M., 2013. Production of low-cost adsorbents with tunable surface chemistry by conjunction of hydrothermal carbonization and activation processes. Microporous Mesoporous Mater. 165, 127–133.
Rouquerol, F., Rouquerol, J., Sing, K., 1999. CHAPTER 1-Introduction. In: Adsorption by Powders and Porous Solids. Academic Press, pp. 1–26.
Saputra, A., Swantomo, D., Ariyanto, T., Sulistyo, H., 2019. Uranium removal from wastewater using $Mg(OH)_2$-Impregnated activated carbon. Water, air. Soil Pollut. 230, 213.
Schettino Junior, M.Â., 2004. Ativação química do carvão de casca de Arroz Utilizando NaOH. Programa Pós Grad. em Física Univerisdade Fed. do Espírito St.
Sing, K.S.W., 1985. Reporting physisorption data for gas/solid systems with special reference to the determination of surface area and porosity (Recommendations 1984). Pure Appl. Chem. 57, 603–619.
Teixeira, V.G., Coutinho, F., Gomes, A.S., 2001. Principais métodos de caracterização da porosidade de resinas à base de divinilbenzeno. Quim. Nova 24, 808–818.
Teng, D., Zhang, B., Xu, G., Wang, B., Mao, K., Wang, J., Sun, J., Feng, X., Yang, Z., Zhang, H., 2020. Efficient removal of Cd (II) from aqueous solution by pinecone biochar: sorption performance and governing mechanisms. Environ. Pollut. 265.
Thommes, M., 2010. Physical adsorption characterization of nanoporous materials. Chemie Ing. Tech 82, 1059–1073.
Thommes, M., Kaneko, K., Neimark, A.V., Olivier, J.P., Rodriguez-Reinoso, F., Rouquerol, J., Sing, K.S.W., 2015. Physisorption of gases, with special reference to the evaluation of surface area and pore size distribution (IUPAC Technical Report). Pure Appl. Chem. 87, 1051–1069.
Thommes, M., Morell, J., Cychosz, K.A., Fröba, M., 2013. Combining nitrogen, argon, and water adsorption for advanced characterization of ordered mesoporous carbons (CMKs) and periodic mesoporous organosilicas (PMOs). Langmuir 29, 14893–14902.
Trakal, L., Sigut, R., Sillerová, H., Faturíková, D., Komárek, M., 2014. Copper removal from aqueous solution using biochar: effect of chemical activation. Arab. J. Chem. 7, 43–52.
Vieira, L.C., de Araujo, L.G., de Padua Ferreira, R.V., da Silva, E.A., Canevesi, R.L.S., Marumo, J.T., 2019. Uranium biosorption by *lemna* sp. and *Pistia stratiotes*. J. Environ. Radioact. 203, 179–186.
Wang, J., Kaskel, S., 2012. KOH activation of carbon-based materials for energy storage. J. Mater. Chem. 22, 23710–23725.
Wu, L., Zhang, S., Wang, J., Ding, X., 2020. Phosphorus retention using iron (II/III) modified biochar in saline-alkaline soils: adsorption, column and field tests. Environ. Pollut. 261, 114223.
Xiong, X., Liu, X., Iris, K.M., Wang, L., Zhou, J., Sun, X., Rinklebe, J., Shaheen, S.M., Ok, Y.S., Lin, Z., Tsang, D.C., 2019. Potentially toxic elements in solid waste streams: fate and management approaches. Environ. Pollut. 253, 680–707.
Yang, R.T., 2013. Gas Separation by Adsorption Processes. Butterworth-Heinemann.
Zhang, Z., Cao, X., Liang, P., Liu, Y., 2013. Adsorption of uranium from aqueous solution using biochar produced by hydrothermal carbonization. J. Radioanal. Nucl. Chem. 295, 1201–1208.
Zhang, J., Shao, J., Jin, Q., Li, Z., Zhang, X., Chen, Y., Zhang, S., Chen, H., 2019. Sludge-based biochar activation to enhance Pb (II) adsorption. Fuel 252, 101–108.